fibers

MDPI

Article

Degradation of Interfacial Bond for FRPs Near-Surface Mounted to Concrete Under Fatigue: An Analytical Approach

Xun Wang [1] and Lijuan Cheng [2,*]

[1] CHEC USA Inc., San Ramon, CA 94583, USA; wangxun34@gmail.com
[2] Department of Civil and Environmental Engineering, University of California-Davis, One Shields Ave., Davis, CA 95616, USA
* Correspondence: dawcheng@ucdavis.edu; Tel.: +1-530-754-8030; Fax: +1-530-752-7872

Abstract: In this study, an analytical model was developed for the local bond degradation behavior between a near-surface mounted (NSM) fiber-reinforced polymer (FRP) and concrete under fatigue loading. A trilinear local bond stress–slip relationship was adopted to characterize the fundamental bond behavior at the FRP-epoxy-concrete interface at different stages of elastic, softening and debonding. A series of post-fatigue direct pull-out tests (DPTs) of NSM FRP-bonded concrete blocks was conducted to provide the local bond degradation laws for the analytical model. The bond region was discretized into finite elements to include the effect of bond degradation to different extents, and a closed-form solution was derived by virtue of appropriate boundary conditions in each fatigue cycle. The model is capable of predicting the FRP strain distribution, local bond stress distribution and relative slip development at a targeted number of fatigue cycles. The reliability of the analytical model was confirmed by experimental data, and its sensitivity to various parameters such as local bond strength, the residual bond strength ratio and Young's modulus of FRP reinforcement was also assessed in this study.

Keywords: polymer matrix composites (PMCs); fatigue; fiber/matrix bond; analytical modeling; near-surface mounted (NSM)

check for updates

Academic Editor: Luciano Ombres

Received: 30 October 2024
Revised: 5 December 2024
Accepted: 7 January 2025
Published: 15 January 2025

Citation: Wang, X.; Cheng, L. Degradation of Interfacial Bond for FRPs Near-Surface Mounted to Concrete Under Fatigue: An Analytical Approach. *Fibers* **2025**, *13*, 9. https://doi.org/10.3390/fib13010009

Copyright: © 2025 by the authors. Licensee MDPI, Basel, Switzerland. This article is an open access article distributed under the terms and conditions of the Creative Commons Attribution (CC BY) license (https://creativecommons.org/licenses/by/4.0/).

1. Introduction

The near-surface mounted (NSM) technique using fiber-reinforced polymer (FRP) composites has been a promising approach to increase the load-carrying capacity of the existing concrete structures, which are substandard according to the current specifications. Its major advantages include but are not limited to the following: (1) faster installation due to the reduced work of surface preparation; (2) being less prone to debonding failure, which leads to a more efficient use of FRP material; and (3) better resistance to environmental corrosion and less visual impact [1,2]. Up to date, extensive research has been conducted focusing on either the bond performance of NSM FRP-adhesive-concrete joints [3–7] or the structural response of strengthened beams, columns, slabs or walls, etc., which is subject to various load cases [8–12].

For NSM-strengthened concrete bridges, cyclic fatigue plays an important role in the structure's service life due to the moving vehicle loads that cause microcracks at the interface between FRPs and epoxy adhesive. This damage progressively accumulates and can finally lead to a failure [13–15]. Quattlebaum et al. [16] conducted a three-point bending test for FRP retrofitted beams under both monotonic and fatigue loading. The NSM technique was shown to significantly increase the flexural strength of the beam, which also outperformed the one using externally bonded reinforcement (EBR) under fatigue without

any debonding. Similar conclusions were also obtained by other independent experimental studies aiming at examining the efficiency of NSM FRPs to extend the service life of beams under fatigue [17–19]. Badawi and Soudki [20] proposed a fatigue prediction model for NSM FRP retrofitted concrete beams based on a strain life approach, assuming the fatigue failure occurred only by the fracture of steel reinforcement. Wahab et al. [21] investigated the influence on the bond fatigue behavior of concrete beams due to the presence of internal steel reinforcement and the surface treatment of NSM CFRP rods. It was found that the bond failure mechanism for beams was not significantly affected by these parameters although beams strengthened by sand-blasted rods showed better fatigue performance than those using spirally wound rods. Oudah and El-Hacha [22] explored the contribution by a prestressed NSM CFRP strip to the performance of the beam under fatigue loading. Their test results indicated that the debonding resistance at the epoxy–concrete interface was enhanced by the increased prestress level.

Although these studies widely focused on the fatigue behavior of NSM FRP-strengthened concrete beams, fewer research studies have been reported on the essential bond performance and degradation of NSM FRP in concrete under fatigue loading. Chen and Cheng [23] conducted a series of direct pull-out tests (DPTs) for NSM FRP-adhesive-concrete joints and proposed a local bond degradation law for both CFRP rod and strip specimens. Al-Saadi and Al-Mahaidi [24] investigated the effect due to NSM CFRP strip dimensions, surface treatment, and the fatigue load range on the fatigue life of concrete specimens. They also proposed a series of load range versus fatigue life equations based on regression analyses. Another systematic study conducted more recently on fatigue included parameters of FRP cross-sectional shapes, surface treatment, and epoxy adhesive types [25]. Although some general bond models have been attempted for a laminated FRP-to-concrete interface [26,27], Chen and Cheng [28] proposed the only analytical fatigue model based on the cohesive zone to predict the fatigue bond behavior of NSM FRP-to-concrete bonded joints. The drawback of this mode is that it was based on a conservative bilinear local bond stress vs. slip relationship, which neglects the mechanical friction between the two debonding layers when the local debonding occurs at the interfaces. It also underestimated the local bond strength of bond regions that were still within the elastic stage during fatigue cycles, which was not in accordance with the recorded test data.

To overcome this drawback, this paper proposes an improved analytical model that is based on a more representative trilinear local bond stress vs. slip relationship considering the post-debonding behavior and the concept of the finite element method (FEM). A series of post-fatigue direct pull-out tests (DPTs) of NSM FRP-bonded concrete blocks was conducted to obtain the local bond degradation laws as well as the residual bond strength within the debonding region of NSM FRP-to-concrete bonded joints. The proposed analytical model is capable of simulating the progression of damaged bond regions and the development of the local bond stress distribution under fatigue loading. Experimental results from direct pull-out tests subject to targeted fatigue cycles were used to verify the reliability of the proposed model, which was followed by a parametric study on the key parameters.

2. Modeling of Bond Degradation Under Fatigue

2.1. Assumptions

The general configuration of a single shear direct pull-out test for the NSM FRP-to-concrete bonded joint is illustrated in Figure 1, where a typical local bond stress distribution including three different bond regions is presented as well. The bond length L is categorized by three different regions: the elastic region ($0 \leq x \leq L–L_d–L_s$), the softening region ($L–L_d–L_s \leq x \leq L–L_d$) and the debonding region ($L–L_d \leq x \leq L$), where x measures the

distance from the free end of the joint; L_s is the softening length; and L_d is the debonding length. Next, apply a one-dimensional mesh to partition the bond length L into the designated number of segments, n_3. n_1 is the total number of segments within the elastic region. (n_2–n_1) represents the total number of segments within the softening region, and (n_3–n_2) is the total number of segments within the debonding region [Figure 2a]. The number of elements of different regions is intended for controlling the accuracy of the analysis. As a result, the length for each element is not identical for different regions and will further be updated upon each fatigue cycle.

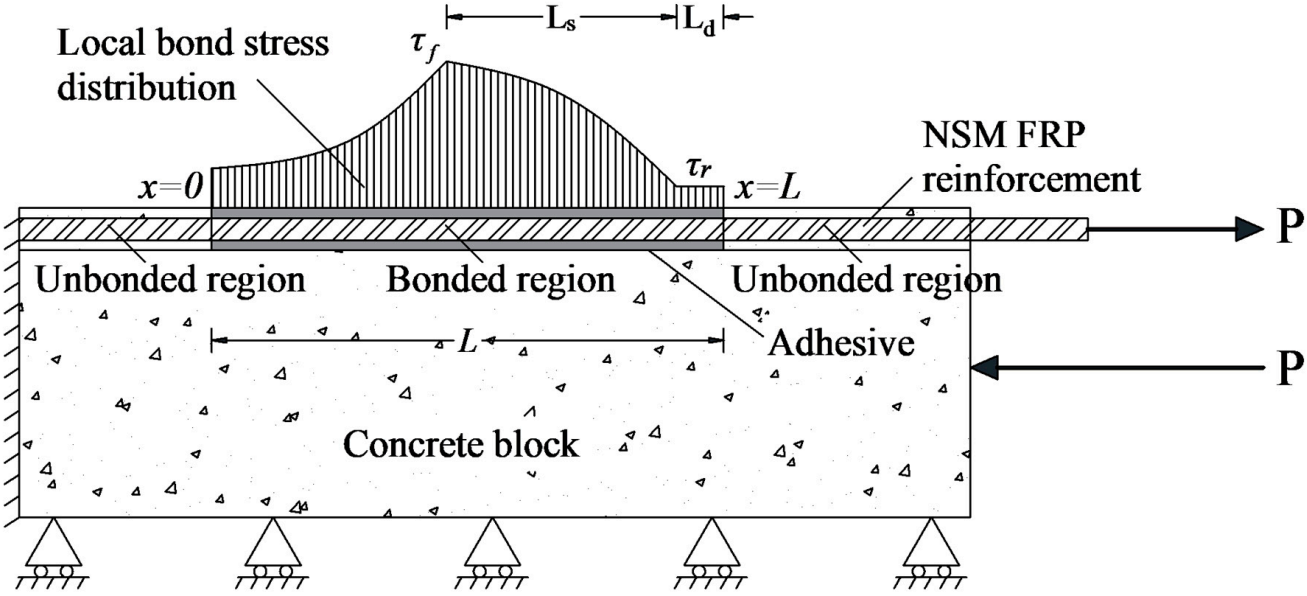


Figure 1. Single shear DPT configuration for NSM FRP-to-concrete bonded joint under pull-out force.

The following important assumptions are introduced to insure the validity of the analytical model:

1. Both the FRP reinforcement and concrete are homogenous and linear elastic. The linear elastic assumption for concrete is based on the experimental observations of this type of joint specimens under DPTs where no significant damage was found in concrete subjected to fatigue cycles up to failure [23,25];
2. The axial stress is uniformly distributed along the cross-section of the FRP reinforcement and the concrete block;
3. The epoxy adhesive is homogeneous, linear elastic and constant in dimensions along the bond length, and it transfers load from the FRP reinforcement to the surrounding concrete as a media. Thus, the thickness of epoxy adhesive is neglected;
4. The bending or twisting effect is neglected in the analysis; i.e., the bond region is subject to pure tension;
5. The NSM bonded joint usually has a weak bond at the interface between the FRP and epoxy adhesive as observed in several experiments [23], particularly for FRP reinforcements without solid surface treatments, and, therefore, it is considered the failure plane;
6. The local bond stress of each bond finite element within the elastic region follows the trilinear local bond slip–stress model as presented in Figure 3 with no degradation. However, for those bond finite elements within the softening region under the current fatigue cycle, of which the relative slip δ between the FRP reinforcement and concrete block increases beyond δ_1, their local bond strength τ_f and the residual bond strength

τ_r will degrade during the following fatigue cycles in accordance with empirical equations. Details will be elaborated in a later section.

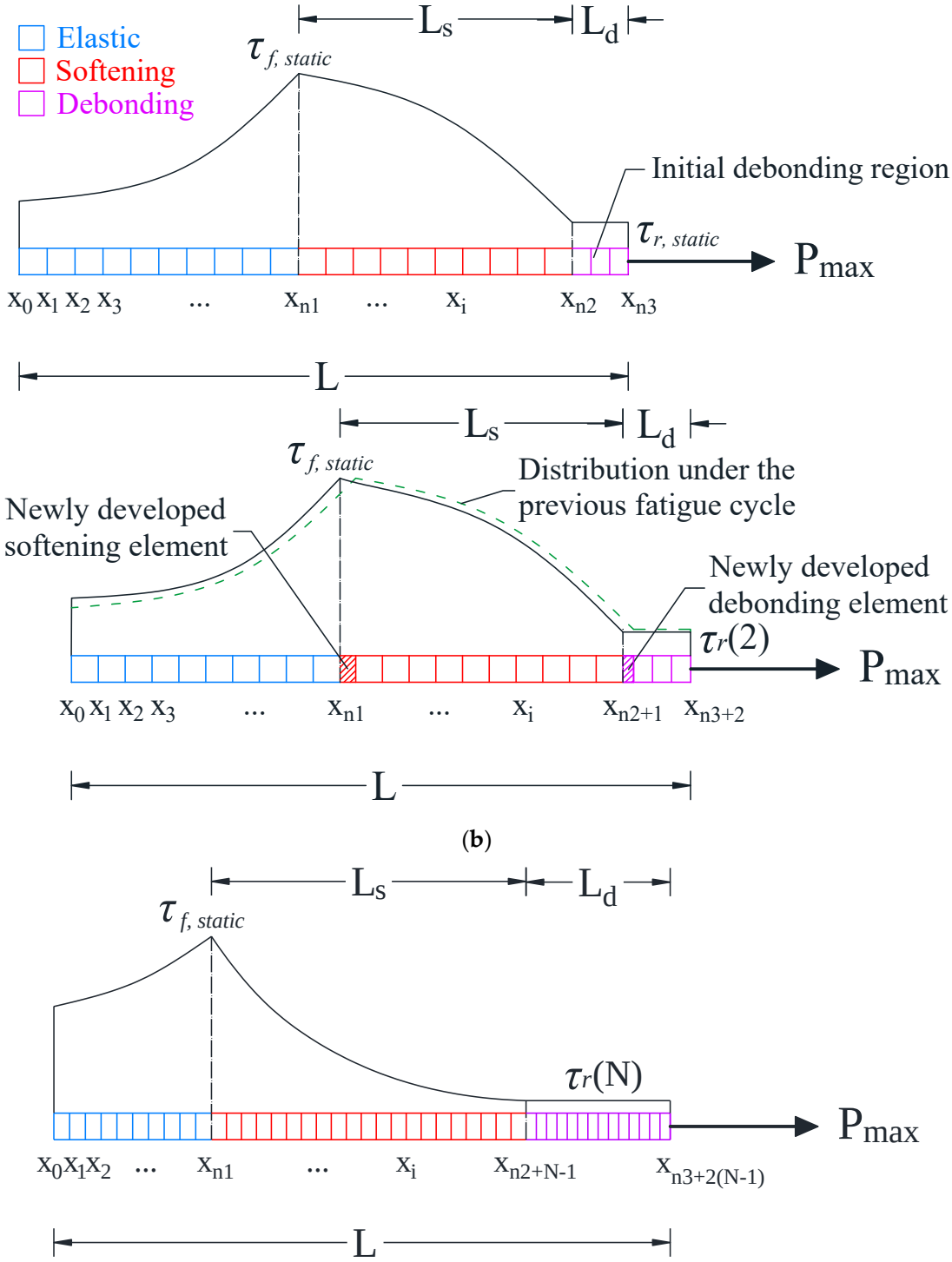


Figure 2. Illustration of the analytical model for the NSM FRP-to-concrete bonded joint under fatigue cycles: (**a**) local bond stress distribution and the bond finite element under the 1st fatigue cycle; (**b**) local bond stress distribution and the bond finite element under the 2nd fatigue cycle; and (**c**) local bond stress distribution and the bond finite element at the *N*th fatigue cycle.

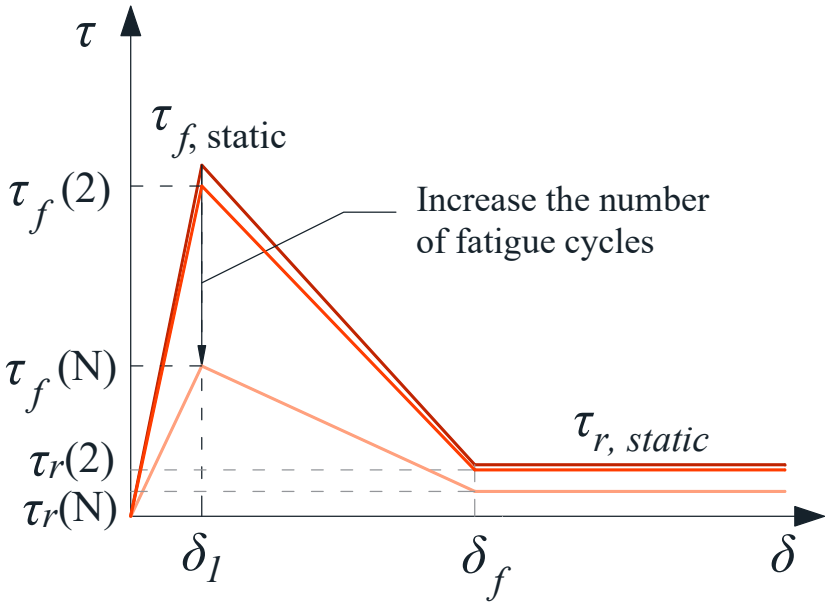


Figure 3. Trilinear local bond stress–slip model under both static and fatigue loading.

2.2. Bond Evolvement Under Fatigue Loading

The concept of adopting the FEM to simulate the local bond degradation under fatigue cycles is illustrated in Figure 2. At the first cycle of fatigue load, three bond regions (elastic, softening and debonding) are developed to balance the maximum applied fatigue load (P_{max}). It should be noted that the local bond stress distribution depends on the magnitude of P_{max}. Based on the assumptions previously defined, if P_{max} is too low to develop the softening region on the bond line, no degradation will even occur, ending up with an infinite fatigue life. Herein, a sufficiently large magnitude of P_{max} is assumed to create the representative three-region local bond distribution for a conceptual illustration. Under the applied P_{max}, a total number of finite elements (n_3) is created in conjunction with (n_3 + 1) nodes, detonated by x_0, x_1, x_2, . . ., x_{n3}, among which x_{n1} is the boundary between the elastic and softening region, and x_{n2} is the boundary between the softening and debonding region. During the next fatigue cycle, damages start for elements from both the softening and debonding regions during the unloading and loading processes, and their local bond stress will slightly drop accordingly, as shown by the dashed line in Figure 2b. To compensate for the loss of local bond stress within these degraded regions and to resist the same P_{max}, the elastic region is further developed with a larger relative slip and a higher local bond stress. As a result, one more softening element will be generated to the right of x_{n1} because its relative slip δ increases and becomes larger than δ_1. Meanwhile, the peak local bond stress distribution ($\tau_{f,static}$) will move towards the left. Similarly, another debonding element will be generated to the right of x_{n2} because its relative slip δ grows and becomes larger than δ_f. This same procedure repeats during the next fatigue cycle, while the peak local bond stress keeps migrating towards the free end until it reaches the critical situation where the residual bond capacity is unable to resist P_{max}, leading to the final fatigue failure of the bond [Figure 2c]. The advantage of applying the FEM here is that each bond element can be simulated independently while following the same degradation law of the NSM FRP-to-concrete bonded joint under fatigue loading.

2.3. Degradation of Local Bond Strength

The local bond stress–slip relationship plays a critical role in the full-range bond behavior of NSM bonded joint under applied loads. A considerable number of studies have already been conducted to obtain this fundamental relationship, and various models have

been proposed, including both linear [27–31] and nonlinear [32,33] categories. Among these models, the bilinear model has been widely adopted to predict the local bond behavior and the load-carrying capacity of NSM bonded joints [23,27,31]. However, an independent experimental study conducted by the author's group [34] confirmed the advantage of adopting a trilinear model because it is more representative of the test results. To this end, the trilinear model (as illustrated in Figure 3) is adopted in this study to predict the local bond behavior under fatigue cycles, as presented in the following equation set:

$$\tau(\delta) = \begin{cases} \frac{\delta}{\delta_1}{\tau_f}^i(N) & for\ 0 \le \delta \le \delta_1\ (a) \\ \frac{\delta_f - \delta}{\delta_f - \delta_1}\left[{\tau_f}^i(N) - {\tau_r}^i(N)\right] + {\tau_r}^i(N) & for\ \delta_1 < \delta \le \delta_f\ (b) \\ {\tau_r}^i(N) & for\ \delta > \delta_f\ (c) \end{cases} \quad (1)$$

where ${\tau_f}^i(N)$ = local bond strength for the ith finite element at the Nth fatigue cycle; ${\tau_r}^i(N)$ = residual local bond strength for the ith finite element at the Nth fatigue cycle; δ_1 = relative slip corresponding to the local bond strength; and δ_f = relative slip at debonding.

On the other hand, several experimental studies [23,25] have verified the gradual degradation of the local bond strength during fatigue cycles as a result of accumulated interfacial damage between the FRP and epoxy adhesive. In addition to the typical static and fatigue direct pull-out tests of the NSM FRP-to-concrete bonded joint, an extra series of fatigue tests using the same test setup [25,34] was conducted in this research to measure the post-fatigue local bond strength (τ_f) of specimens after 10, 100, 1000, and 10,000 fatigue cycles, respectively. The test setup involved positioning the concrete specimens vertically and pulling the embedded NSM reinforcement encased in steel tubes that were clamped in the steel jaw on the hydraulic head of the actuator with a built-in load cell. These post-fatigue bond strengths of the selected test specimens [34] are entered in Tables 1 and 2 (last two columns) for CFRP rod and strip specimens, respectively, in conjunction with their static counterparts and fatigue life sets. The fatigue life sets were tested either to fatigue failure or a threshold fatigue cycle, e.g., one million cycles or two million cycles, due to the practical time constraints of the experiment. The specimens of the latter ones were then statically loaded up to failure in a direct pull-out test setup to measure their remaining bond capacities, e.g., the specimen set R-SCSW-A1-1060-F-N. According to the test results in Tables 1 and 2, the post-fatigue local bond strength τ_f shows a declining tendency for both CFRP rod and strip specimens. The average bond strength τ_{avg} is defined as the pull-out force P_f divided by the bond surface area of the NSM FRP reinforcement (i.e., the bond length multiplied by the perimeter of the cross-section of the NSM FRP reinforcement). This average bond strength τ_{avg} is relatively stable under all fatigue cycle cases. Note that the average bond strength τ_{avg} adopted in this paper aims at comparing the global bond performance of tested specimens under the same calculation basis, regardless of the actual failure mode. For example, the failure mode of specimen set R-SCSW-A1-N was primarily concrete and epoxy breakage, but interfacial debonding between the FRP rod and the epoxy adhesive was also observed for most of its fatigue counterparts. On the other hand, specimens using strips were mostly failed by interfacial debonding between the FRP strip and the epoxy adhesive [25,34].

To quantify the local bond degradation, logarithmic functions with a base of 10 are adopted to correlate the normalized local bond strength $\tau_f(N)$ (with respect to the static local bond strength $\tau_{f,static}$) to the fatigue cycle N for both cases [Figures 4a and 5a]. Based on the regression analysis of these test data, Equations (2) and (4) below are obtained and proposed for the empirical degradation laws for the local bond strength of CFRP rod and strip cases, with a R^2 value of 0.9595 and 0.9507, respectively. It should be noted that

the very last data point on the plot in Figure 4a was actually the average bond strength τ_{avg} obtained from the post-fatigue direct pull-out test of the rod specimens due to the damaged strain gauges at large fatigue cycles. The same applies to Figure 5a for the strip specimens, where the last data point was obtained from the strain gauge readings in the last few cycles before fatigue failure for the strip specimens because the post-fatigue tests were not applicable for these specimens.

Table 1. Test results of CFRP rod specimens for local bond degradation.

ID [a]	Fatigue Life	Static or Post-Fatigue Pull-Out Force P_f (kN)		Average Bond Strength τ_{avg} (MPa)		Static or Post-Fatigue Local Bond Strength τ_f (MPa)	
		Value	Average	Value	Average	Value	Average
R-SCSW-A1-N-1	– [b]	64.81		8.69		15.76	
R-SCSW-A1-N-2	–	90.39	78.54	12.11	10.53	17.43	17.30
R-SCSW-A1-N-3	–	80.42		10.78		18.70	
R-SCSW-A1-1060-1E1-N-1	–	84.15		11.28		16.85	
R-SCSW-A1-1060-1E1-N-2	–	81.56	83.07	10.93	11.13	17.37	17.16
R-SCSW-A1-1060-1E1-N-3	–	83.50		11.19		17.27	
R-SCSW-A1-1060-1E2-N-1	–	106.60		14.29		16.03	
R-SCSW-A1-1060-1E2-N-2	–	90.09	93.28	12.07	12.50	8.52	14.93
R-SCSW-A1-1060-1E2-N-3	–	83.15		11.14		20.22	
R-SCSW-A1-1060-1E3-N-1	–	78.69		10.55		14.37	
R-SCSW-A1-1060-1E3-N-2	–	94.78	86.68	12.70	11.62	9.76	14.06
R-SCSW-A1-1060-1E3-N-3	–	86.58		11.60		18.05	
R-SCSW-A1-1060-1E4-N-1	–	91.93		12.32		8.78	
R-SCSW-A1-1060-1E4-N-2	–	91.65	94.17	12.28	12.62	15.99	12.41
R-SCSW-A1-1060-1E4-N-3	–	98.93		13.26		12.47	
R-SCSW-A1-1060-F-N-1 [c]	2,000,000	80.42		10.78		– [d]	
R-SCSW-A1-1060-F-N-2	1,000,000	83.17	82.26	11.15	11.02	–	–
R-SCSW-A1-1060-F-N-3	1,000,000	83.19		11.15		–	

[a] CFRP rod specimen (R) with a sand-coated and spirally wound (SCSW) surface, adhesive type A1 (Pak CF), normal weight concrete (N), additionally undergoing a cyclic load range of 10–60% of the corresponding static capacity (1060) and being tested up to a specific number of fatigue cycles (1E1, 1E2, 1E3, 1E4) or failure (F) for fatigue specimens; [b] not applicable because the specimen was not tested up to fatigue failure; and [c] the first attempt to obtain the real fatigue life of the specimen. Since no obvious deterioration was observed up to two million cycles, the upper limit was then changed to one million cycles for the rest of the specimens; [d] Not applicable due to damaged strain gauges.

$$\frac{\tau_f(N)}{\tau_{f,static}} = -0.0629 \log_{10}(N) + 1 \text{ for CFRP rod specimens} \quad (2)$$

$$\frac{\tau_r(N)}{\tau_{r,static}} = -0.1449 \log_{10}(N) + 1 \text{ for CFRP rod specimens} \quad (3)$$

$$\frac{\tau_f(N)}{\tau_{f,static}} = -0.1226 \log_{10}(N) + 1 \text{ for CFRP strip specimens} \quad (4)$$

$$\frac{\tau_r(N)}{\tau_{r,static}} = -(N-1)/969084 + 1 \text{ for CFRP strip specimens} \quad (5)$$

Due to the fact that two of the strain gauges within the debonding region were damaged during various fatigue cycles, the residual bond strength was not directly measurable from the test data. The analytical degradation laws, represented by Equations (3) and (5) for the rod and strip cases, respectively, were thus proposed through a trial-and-error method based on the principle that the characteristics of the observed local bond stress development can be reasonably captured by the proposed analytical model (to be discussed

next). For the normalized residual bond strength $\tau_r(N)/\tau_{r,static}$, a logarithmic function is also used for the CFRP rod specimens [Figure 4b], and a linear function is adopted for the CFRP strip specimens [Figure 5b].

Table 2. Test results of CFRP strip specimens for local bond degradation.

ID [a]	Fatigue Life	Static or Post-Fatigue Pull-Out Force P_f (kN)		Average Bond Strength τ_{avg} (MPa)		Static or Post-Fatigue Local Bond Strength τ_f (MPa)	
		Value	Average	Value	Average	Value	Average
S-RO-A1-N-1	– [b]	51.62		5.04		10.31	
S-RO-A1-N-2	–	62.92	54.39	6.14	5.31	10.88	10.42
S-RO-A1-N-3	–	48.62		4.74		10.07	
S-RO-A1-1060-1E1-N-1	–	43.47		4.24		6.31	
S-RO-A1-1060-1E1-N-2	–	65.44	62.20	6.38	6.07	8.55	8.26
S-RO-A1-1060-1E1-N-3	–	77.69		7.58		9.93	
S-RO-A1-1060-1E2-N-1	–	62.85		6.13		7.57	
S-RO-A1-1060-1E2-N-2	–	40.23	55.38	3.93	5.40	5.16	7.24
S-RO-A1-1060-1E2-N-3	–	63.05		6.15		8.99	
S-RO-A1-1060-1E3-N-1	–	61.62		6.01		6.88	
S-RO-A1-1060-1E3-N-2 [c]	–		57.38		5.60		6.54
S-RO-A1-1060-1E3-N-3	–	53.13		5.18		6.20	
S-RO-A1-1060-1E4-N-1	–	48.08		4.69		5.61	
S-RO-A1-1060-1E4-N-2	–	50.95	56.39	4.97	5.50	5.04	5.98
S-RO-A1-1060-1E4-N-3	–	70.15		6.84		7.30	
S-RO-A1-1060-F-N-1 [d]		– [e]		–		–	
S-RO-A1-1060-F-N-2	850,340	–	–	–	–	–	–
S-RO-A1-1060-F-N-3	1,087,829	–		–		–	

[a] CFRP strip specimen (S) with a roughened (RO) surface, adhesive type A1 (Pak CF), normal weight concrete (N), additionally undergoing a cyclic load range of 10–60% of the corresponding static capacity (1060) and being tested up to a specific number of fatigue cycles (1E1, 1E2, 1E3, 1E4) or failure (F) for fatigue specimens; [b] not applicable because the specimen was not tested up to fatigue failure; [c] not included because it failed in a different mechanism with both the concrete and epoxy damaged, which results in an unexpected high pull-out force; [d] not included since the specimen failed prematurely by delamination of the CFRP top surface; and [e] not applicable due to damaged strain gauges.

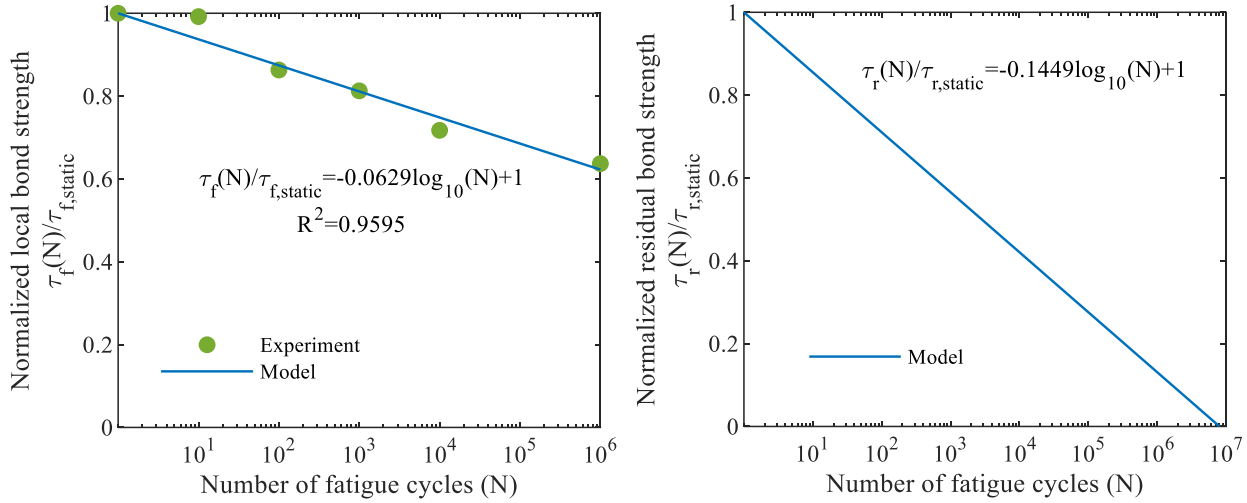


Figure 4. Local bond degradation law for CFRP rod specimens: (**a**) local bond strength; and (**b**) residual bond strength.

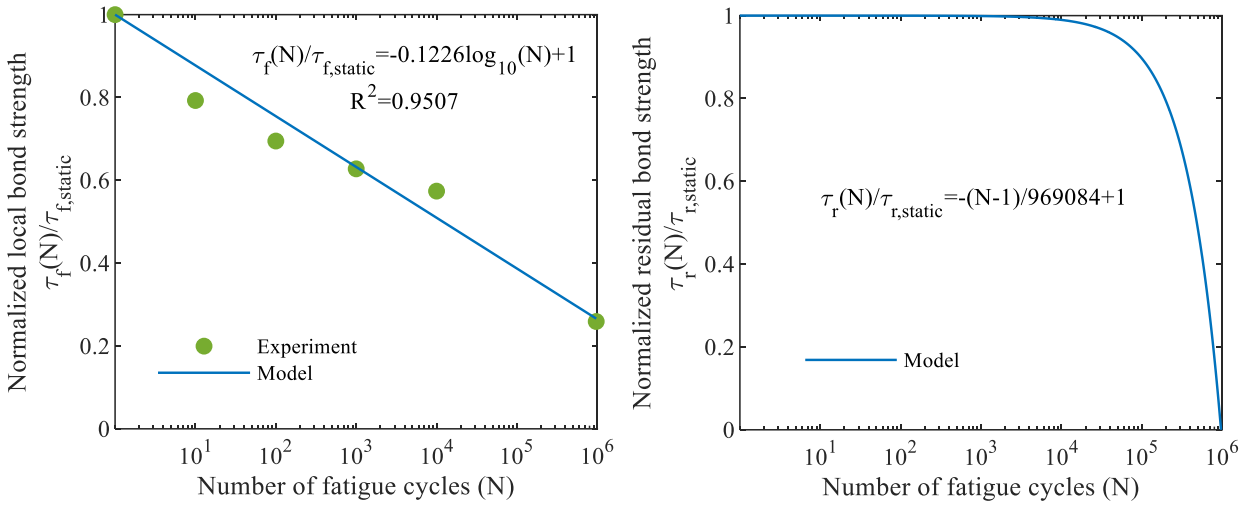


Figure 5. Local bond degradation law for CFRP strip specimens: (**a**) local bond strength; and (**b**) residual bond strength.

2.4. Governing Equation and General Solutions

Although the bond line is discretized into finite elements, the fundamental interactions within the NSM FRP-adhesive-concrete joint remain the same as the ones introduced in the analytical model [27]. Thus, the governing equation for the *i*th finite element can be represented by the following general differential equation regardless of the bond region to which it belongs:

$$\frac{d^2\delta}{dx^2} - \lambda^2\tau_i(\delta) = 0 \quad for\ x_{i-1} \le x \le x_i \tag{6}$$

where

$$\lambda = \sqrt{L_p\left(\frac{1}{A_fE_f} + \frac{1}{A_cE_c}\right)} \tag{7}$$

in which A_f = cross-sectional area of the NSM FRP reinforcement; E_f = Young's modulus of the NSM FRP reinforcement; A_c = cross-sectional area of the concrete block; E_c = Young's modulus of the concrete block; L_p = perimeter of the failure plane; $\tau_i(\delta)$ = local bond stress–slip relationship for the *i*th finite element; and x_{i-1}, x_i = start and end coordinate of the *i*th element where $x_0 = 0$ (free end of the bond line).

The theoretical solutions to this governing equation depend on the type of bond finite elements, including elastic, softening and debonding as illustrated in Figure 2a. These solutions are derived separately as follows:

(a) For elements within the elastic region ($0 \le x \le L–L_d–L_s$), the general solution can be obtained by firstly substituting Equation (1a) into Equation (6), which yields the following equation:

$$\frac{d^2\delta}{dx^2} - \left({\lambda_1}^i\right)^2\delta = 0 \tag{8}$$

where

$${\lambda_1}^i = \sqrt{\frac{{\tau_f}^i}{\delta_1}L_p\left(\frac{1}{A_fE_f} + \frac{1}{A_cE_c}\right)} \tag{9}$$

The relative slip δ can be further derived by solving this homogeneous linear second-order ordinary differential equation (ODE) as given below:

$$\delta = {C_1}^i\cosh\left({\lambda_1}^i x\right) + {C_2}^i\sinh\left({\lambda_1}^i x\right) \tag{10}$$

Then, the local bond stress τ and the FRP stress σ_f can be easily obtained as follows:

$$\tau = \frac{{\tau_f}^i}{\delta_1}\left[{C_1}^i \cosh\left({\lambda_1}^i x\right) + {C_2}^i \sinh\left({\lambda_1}^i x\right)\right] \tag{11}$$

$$\sigma_f = \frac{L_p {\tau_f}^i}{A_f \delta_1 {\lambda_1}^i}\left[{C_1}^i \sinh\left({\lambda_1}^i x\right) + {C_2}^i \cosh\left({\lambda_1}^i x\right)\right] + {C_3}^i \tag{12}$$

where ${C_1}^i$, ${C_2}^i$ and ${C_3}^i$ = constants of the ith element that remain to be solved by boundary conditions.

(b) For elements within the softening region (L–L_d–$L_s \le x \le L$–L_d), the general equation of relative slip δ can be derived similarly by solving the following nonhomogeneous ODE, which is obtained by substituting Equation (1b) into Equation (6) as follows:

$$\frac{d^2\delta}{dx^2} + \left({\lambda_2}^i\right)^2 \delta = \frac{\delta_f {\tau_f}^i - \delta_1 {\tau_r}^i}{\delta_f - \delta_1}\lambda^2 \tag{13}$$

where

$${\lambda_2}^i = \sqrt{\frac{{\tau_f}^i - {\tau_r}^i}{\delta_f - \delta_1} L_p \left(\frac{1}{A_f E_f} + \frac{1}{A_c E_c}\right)} \tag{14}$$

The explicit solution to Equation (13) is hence derived as follows:

$$\delta = {C_1}^i \cos\left[{\lambda_2}^i (x - L + L_d + L_s)\right] + {C_2}^i \sin\left[{\lambda_2}^i (x - L + L_d + L_s)\right] + \frac{\delta_f {\tau_f}^i - \delta_1 {\tau_r}^i}{{\tau_f}^i - {\tau_r}^i} \tag{15}$$

Then, the local bond stress τ and the FRP stress σ_f can be obtained as follows:

$$\tau = -\frac{{\tau_f}^i - {\tau_r}^i}{\delta_f - \delta_1}\left\{{C_1}^i \cos\left[{\lambda_2}^i (x - L + L_d + L_s)\right] + {C_2}^i \sin\left[{\lambda_2}^i (x - L + L_d + L_s)\right]\right\} \tag{16}$$

$$\sigma_f = -\frac{L_p\left({\tau_f}^i - {\tau_r}^i\right)}{A_f\left(\delta_f - \delta_1\right){\lambda_2}^i}\left\{{C_1}^i \sin\left[{\lambda_2}^i (x - L + L_d + L_s)\right] - {C_2}^i \cos\left[{\lambda_2}^i (x - L + L_d + L_s)\right]\right\} + {C_3}^i \tag{17}$$

(c) For elements within the debonding region (L–$L_d \le x \le L$), the same procedure is applied by substituting Equation (1c) into Equation (6) yielding the following:

$$\frac{d^2\delta}{dx^2} = {\lambda_3}^i \tag{18}$$

where

$$\lambda_3 = {\tau_r}^i L_p \left(\frac{1}{A_f E_f} + \frac{1}{A_c E_c}\right) \tag{19}$$

Thus, the general solution of the relative slip δ, the local bond stress τ and the FRP stress σ_f are obtained as follows:

$$\delta = 0.5{\lambda_3}^i x^2 + {C_1}^i x + {C_2}^i \tag{20}$$

$$\tau = {\tau_r}^i \tag{21}$$

$$\sigma_f = \frac{L_p}{A_f}{\tau_r}^i x + {C_3}^i \tag{22}$$

2.5. Boundary Conditions

For a total number of n finite elements on the bond line, $3n$ unknown constants (${C_1}^i$, ${C_2}^i$ and ${C_3}^i$, i = 1, 2, …, n) need to be determined to obtain the complete solutions of the relative slip δ, the local bond stress τ and the FRP stress σ_f. In addition, both the softening length L_s and the debonding length L_d are unknown under the applied fatigue load P_{max}, which add up the total unknown constants to $(3n + 2)$. In terms of the internal continuity among these finite elements, the relative slip δ, the first derivative of δ, and the FRP stress σ_f are required to remain continuous at the node between two neighboring elements. On the other hand, the external boundary conditions are required to be satisfied at both the free and loaded end.

The internal boundary conditions are presented as follows, where the three equations in each category represent the internal continuity of the relative slip δ, the first derivative of δ, and the FRP stress σ_f, respectively:

(a) For interior nodes of the elastic region ($0 < x < L–L_d–L_s$),

$$C_1{}^i \cosh\left(\lambda_1{}^i x_i\right) + C_2{}^i \sinh\left(\lambda_1{}^i x_i\right) = C_1{}^{i+1} \cosh\left(\lambda_1{}^{i+1} x_i\right) + C_2{}^{i+1} \sinh\left(\lambda_1{}^{i+1} x_i\right) \quad (23)$$

$$C_1{}^i \lambda_1{}^i \sinh\left(\lambda_1{}^i x_i\right) + C_2{}^i \lambda_1{}^i \cosh\left(\lambda_1{}^i x_i\right) = C_1{}^{i+1} \lambda_1{}^{i+1} \sin\left(\lambda_1{}^{i+1} x_i\right) + C_2{}^{i+1} \lambda_1{}^{i+1} \cosh\left(\lambda_1{}^{i+1} x_i\right) \quad (24)$$

$$\begin{aligned} &\frac{L_p {\tau_f}^i}{A_f \delta_1 {\lambda_1}^i}\left[C_1{}^i \sinh\left(\lambda_1{}^i x_i\right) + C_2{}^i \cosh\left(\lambda_1{}^i x_i\right)\right] + C_3{}^i \\ &= \frac{L_p {\tau_f}^{i+1}}{A_f \delta_1 {\lambda_1}^{i+1}}\left[C_1{}^{i+1} \sinh\left(\lambda_1{}^{i+1} x_i\right) + C_2{}^{i+1} \cosh\left(\lambda_1{}^{i+1} x_i\right)\right] + C_3{}^{i+1} \end{aligned} \quad (25)$$

(b) For nodes between the elastic and the softening region ($x = L–L_d–L_s$),

$$\begin{aligned} &C_1{}^{n_1} \cosh[{\lambda_1}^{n_1}(L - L_d - L_s)] + C_2{}^{n_1} \sinh[{\lambda_1}^{n_1}(L - L_d - L_s)] \\ &= C_1{}^{n_1+1} + \frac{\delta_f {\tau_f}^{n_1+1} - \delta_1 {\tau_r}^{n_1+1}}{{\tau_f}^{n_1+1} - {\tau_r}^{n_1+1}} \end{aligned} \quad (26)$$

$$C_1{}^{n_1} {\lambda_1}^{n_1} \sinh[{\lambda_1}^{n_1}(L - L_d - L_s)] + C_2{}^{n_1} {\lambda_1}^{n_1} \cosh[{\lambda_1}^{n_1}(L - L_d - L_s)] = C_2{}^{n_1+1} {\lambda_2}^{n_1+1} \quad (27)$$

$$\begin{aligned} &\frac{L_p {\tau_f}^{n_1}}{A_f \delta_1 {\lambda_1}^{n_1}}\{C_1{}^{n_1} \sinh[{\lambda_1}^{n_1}(L - L_d - L_s)] + C_2{}^{n_1} \cosh[{\lambda_1}^{n_1}(L - L_d - L_s)]\} + C_3{}^{n_1} \\ &= \frac{L_p\left({\tau_f}^{n_1+1} - {\tau_r}^{n_1+1}\right)}{A_f\left(\delta_f - \delta_1\right){\lambda_2}^{n_1+1}} C_2{}^{n_1+1} + C_3{}^{n_1+1} \end{aligned} \quad (28)$$

(c) For interior nodes of the softening region ($L–L_d–L_s < x < L–L_d$),

$$\begin{aligned} &C_1{}^i \cos\left[\lambda_2{}^i(x_i - L + L_d + L_s)\right] + C_2{}^i \sin\left[\lambda_2{}^i(x_i - L + L_d + L_s)\right] + \frac{\delta_f {\tau_f}^i - \delta_1 {\tau_r}^i}{{\tau_f}^i - {\tau_r}^i} \\ &= C_1{}^{i+1} \cos\left[\lambda_2{}^{i+1}(x_i - L + L_d + L_s)\right] + C_2{}^{i+1} \sin\left[\lambda_2{}^{i+1}(x_i - L + L_d + L_s)\right] + \frac{\delta_f {\tau_f}^{i+1} - \delta_1 {\tau_r}^{i+1}}{{\tau_f}^{i+1} - {\tau_r}^{i+1}} \end{aligned} \quad (29)$$

$$\begin{aligned} &-C_1{}^i \lambda_2{}^i \sin\left[\lambda_2{}^i(x_i - L + L_d + L_s)\right] + C_2{}^i \lambda_2{}^i \cos\left[\lambda_2{}^i(x_i - L + L_d + L_s)\right] \\ &= -C_1{}^{i+1} \lambda_2{}^{i+1} \sin\left[\lambda_2{}^{i+1}(x_i - L + L_d + L_s)\right] + C_2{}^{i+1} \lambda_2{}^{i+1} \cos\left[\lambda_2{}^{i+1}(x_i - L + L_d + L_s)\right] \end{aligned} \quad (30)$$

$$\begin{aligned} &-\frac{L_p\left({\tau_f}^i - {\tau_r}^i\right)}{A_f\left(\delta_f - \delta_1\right)\lambda_2{}^i}\left\{C_1{}^i \sin\left[\lambda_2{}^i(x_i - L + L_d + L_s)\right] - C_2{}^i \cos\left[\lambda_2{}^i(x_i - L + L_d + L_s)\right]\right\} + C_3{}^i \\ &= -\frac{L_p\left({\tau_f}^{i+1} - {\tau_r}^{i+1}\right)}{A_f\left(\delta_f - \delta_1\right)\lambda_2{}^{i+1}}\left\{C_1{}^{i+1} \sin\left[\lambda_2{}^{i+1}(x_i - L + L_d + L_s)\right] - C_2{}^{i+1} \cos\left[\lambda_2{}^{i+1}(x_i - L + L_d + L_s)\right]\right\} + C_3{}^{i+1} \end{aligned} \quad (31)$$

(d) For nodes between the softening and the debonding region ($x = L–L_d$) at the Nth fatigue cycle,

$$C_1{}^{n_2+N-1}\cos\left(\lambda_2{}^{n_2+N-1}L_s\right) + C_2{}^{n_2+N-1}\sin\left(\lambda_2{}^{n_2+N-1}L_s\right) + \frac{\delta_f\tau_f{}^{n_2+N-1} - \delta_1\tau_r{}^{n_2+N-1}}{\tau_f{}^{n_2+N-1} - \tau_r{}^{n_2+N-1}} = 0.5\lambda_3{}^{n_2+N}(L-L_d)^2 + C_1{}^{n_2+N}(L-L_d) + C_2{}^{n_2+N} \quad (32)$$

$$-C_1{}^{n_2+N-1}\lambda_2{}^{n_2+N-1}\sin\left(\lambda_2{}^{n_2+N-1}L_s\right) + C_2{}^{n_2+N-1}\lambda_2{}^{n_2+N-1}\cos\left(\lambda_2{}^{n_2+N-1}L_s\right) = \lambda_3{}^{n_2+N}(L-L_d) + C_1{}^{n_2+N} \quad (33)$$

$$-\frac{L_p\left(\tau_f{}^{n_2+N-1} - \tau_r{}^{n_2+N-1}\right)}{A_f\left(\delta_f-\delta_1\right)\lambda_2{}^{n_2+N-1}}\left[C_1{}^{n_2+N-1}\sin\left(\lambda_2{}^{n_2+N-1}L_s\right) - C_2{}^{n_2+N-1}\cos\left(\lambda_2{}^{n_2+N-1}L_s\right)\right] + C_3{}^{n_2+N-1} = \frac{L_p}{A_f}\tau_r{}^{n_2+N}(L-L_d) + C_3{}^{n_2+N} \quad (34)$$

(e) For interior nodes of the debonding region ($L–L_d < x < L$),

$$0.5\lambda_3{}^i x_i{}^2 + C_1{}^i x_i + C_2{}^i = 0.5\lambda_3{}^{i+1}x_i{}^2 + C_1{}^{i+1}x_i + C_2{}^{i+1} \quad (35)$$

$$\lambda_3{}^i x_i + C_1{}^i = \lambda_3{}^{i+1}x_i + C_1{}^{i+1} \quad (36)$$

$$\frac{L_p}{A_f}\tau_r{}^i x_i + C_3{}^i = \frac{L_p}{A_f}\tau_r{}^{i+1}x_i + C_3{}^{i+1} \quad (37)$$

The external boundary conditions to be satisfied at both the free and loaded end are presented as follows:

(a) The FRP stress $\sigma_f = 0$ when $x = 0$:

$$\frac{L_p\tau_f{}^1}{A_f\delta_1\lambda_1{}^1}C_2{}^1 + C_3{}^i = 0 \quad (38)$$

(b) The concrete stress $\sigma_c = 0$ when $x = 0$, which leads to $d\delta/dx = 0$ at the free end:

$$C_2{}^1\lambda_1{}^1 = 0 \quad (39)$$

(c) The relative slip $\delta = \delta_1$ when $x = L–L_d–L_s$:

$$C_1{}^{n_1}\cosh[\lambda_1{}^{n_1}(L-L_d-L_s)] + C_2{}^{n_1}\sinh[\lambda_1{}^{n_1}(L-L_d-L_s)] = \delta_1 \quad (40)$$

(d) The relative slip $\delta = \delta_f$ when $x = L–L_d$ at the Nth fatigue cycle:

$$C_1{}^{n_2+N-1}\cos\left(\lambda_2{}^{n_2+N-1}L_s\right) + C_2{}^{n_2+N-1}\sin\left(\lambda_2{}^{n_2+N-1}L_s\right) + \frac{\delta_f\tau_f{}^{n_2+N-1} - \delta_1\tau_r{}^{n_2+N-1}}{\tau_f{}^{n_2+N-1} - \tau_r{}^{n_2+N-1}} = \delta_f \quad (41)$$

(e) The FRP stress $\sigma_f = P_{max}/A_f$ when $x = L$ at the Nth fatigue cycle:

$$\frac{L_p}{A_f}\tau_r{}^{n_3+2(N-1)}L + C_3{}^{n_3+2(N-1)} = \frac{P_{\max}}{A_f} \quad (42)$$

The total number of the internal boundary conditions described in Equations (23)–(37) is $(3n - 3)$, providing that n finite elements are partitioned within the bond length. In addition, by adding the five external boundary conditions presented in Equations (38)–(42), the total number of independent equations becomes $(3n + 2)$, which equals the number of the unknown constants. However, both the softening length L_s and the debonding length L_d are implicit parameters since all other unknown constants, $C_1{}^i$, $C_2{}^i$ and $C_3{}^i$ ($i = 1, 2, \ldots, n$), are explicitly

solvable via linear algebra on the premise that both L_s and L_d are determined in advance. Therefore, an iteration process in conjunction with a calculation algorithm is necessary to reach converged solutions to the finite element problem.

2.6. Algorithm Framework

The strategy of solving this one-dimensional FEM problem with a changing number of elements, which depends on the number of fatigue cycles, has been streamlined into the following steps with a flow chart illustrated in Figure 6:

1. A slip tolerance T_{slip} and a force tolerance T_{force} are preset to control the convergency of the iteration algorithm. The bond failure limit L_f controls the extent of the bond development towards failure. As expected, a smaller tolerance leads to higher accuracy at the expense of a longer calculating time;
2. Assuming the maximum applied load P_{max} is large enough to develop at least the softening stage of the NSM FRP-to-concrete bonded joint, i.e., $\delta > \delta_1$ at the loaded end, two scenarios are considered: (a) debonding already exists; or (b) debonding does not occur at the first fatigue cycle. These two scenarios can be easily determined by the analytical bond model under the static loading case since no degradation accumulates at the first fatigue cycle. Similarly, both ${L_s}^1$ and ${L_d}^1$ can be determined beforehand at the beginning of the iteration;
3. For both scenarios, the local bond properties of each element, i.e., ${\tau_f}^i$ and ${\tau_r}^i$, will be updated cycle by cycle as per the degradation law described by Equations (2)–(5). It is also important to note that the newly developed elements generated in each cycle, as illustrated in Figure 2b, will have less degradation than those softening or debonding elements that already existed before the current cycle. In principle, both the local bond strength ${\tau_f}^j$ and the residual bond strength ${\tau_r}^i$ of a specific element depend solely on the number of fatigue cycles that this particular element experiences rather than the current number of fatigue cycles;
4. Starting from the second fatigue cycle, an iterative process is required to solve the implicit parameters ${L_s}^k$ and ${L_d}^k$ for scenario (a) and ${L_s}^k$ for scenario (b) under the current kth fatigue cycle. As shown in Figure 6, the force (traction) boundary condition [Equation (42)] and the displacement boundary condition [Equation (41)] are applied to obtain ${L_s}^k$ and ${L_d}^k$, respectively. The speed and accuracy of this iterative process depend mainly on the magnitude of the preset tolerances and the algorithm adopted to update ${L_s}^k$ and ${L_d}^k$ in the iteration. For example, the method of bisection is implemented in this study for its simplicity and good accuracy. For scenario (b), if the displacement boundary condition $\delta > \delta_f$ at the loaded end is reached before the target number of fatigue cycles N, which means the softening stage should be developed, it will be automatically switched to scenario (a) and continues for the next cycle; and
5. The algorithm will provide the FEM solutions, including the relative slip δ, the local bond stress δ and the FRP stress σ_f, etc., along with the bond line at the target number of fatigue cycles N if the NSM FRP joint still survives. Otherwise, the debonding failure and the fatigue life will be obtained whilst the softening length L_s develops all the way to the free end, yet the joint is still unable to balance the applied P_{max}.



Figure 6. Flow chart of the analytical model for the NSM FRP-to-concrete bonded joint.

3. Predictions Using Proposed Model

A Matlab 9.10 subroutine was programmed to create the analytical model based on the trilinear local bond stress–slip relationship and degradation law as previously described. The static bond parameters adopted for the analytical model are summarized in Table 3. Experimental variables such as material properties, the geometric detailing of the NSM FRP-to-concrete bonded joint and the maximum fatigue load P_{max} were obtained from an earlier study [25] as the input parameters of the model, along with the target number of fatigue cycles N and the tolerances of convergency. Analytical predictions of the FRP strain distribution and the local bond stress distribution are illustrated in Figures 7–10, along with the test results for comparisons, for both FRP rod and strip

specimens. Among these plots, comparisons were made at 10, 100, 1000, 10,000 and 100,000 fatigue cycles to present the overall performance of the model during various fatigue cycles. Short abbreviations of specimen designation were used to improve the readability of the plots. For example, R-1E2 represents specimens labeled with R-SCSW-A1-1060-1E2-N (as SCSW-A1-1060 remains constant), and S-F represents specimens S-RO-A1-1060-F-N (as RO-A1-1060 remains constant).

Table 3. Key parameters of the trilinear local bond stress–slip relationship under the static loading case [34].

Parameter	NSM FRP-to-Concrete Bonded Joint	
	CFRP Rod Specimens	CFRP Strip Specimens
$\tau_{f,static}$ (MPa)	17.30	10.42
$\tau_{r,static}$ (MPa)	7.18	3.37
δ_1 (mm)	0.08	0.05
δ_f (mm)	0.45	0.21

Based on the comparisons in these figures, the proposed model generally captures the entire local bond degradation behavior under the fatigue load. As the number of fatigue cycles N increases from 10 [Figures 7a and 9a] to 100,000 [Figures 7e and 9e], the FRP materials from regions near the loaded end progress a higher utilization, which is featured by a flatter distribution of the FRP strain near the loaded end, as shown in both Figures 7 and 9 for rod and strip specimens, respectively. This phenomenon is consistent with the gradual migration of the peak local bond stress towards the free end (away from the loaded end) due to accumulated bond damage within the debonding and softening regions, as seen in Figures 8 and 10 for rod and strip specimens, respectively. It should be noted that the fluctuation of fatigue test results is typically inevitable, leading to certain degrees of scattering. This is mainly due to the difficulty of strain measurements on the embedded NSM FRP (particularly FRP reinforcements with round cross-section and a spirally wound surface) and the sustained friction between the strain gauges and the surrounding epoxy adhesive during fatigue cycles, leading to the early malfunction of strain gauges installed closer to the loaded end. Regardless, the proposed model primarily aims at capturing the bond development behavior of the NSM FRP-to-concrete bonded joint under fatigue cycles as observed in the experiments due to the local bond degradation.

Moreover, the relative slip at the loaded end for representative specimen sets is compared in Figure 11. These selected specimen sets (i.e., R-SCSW-A1-1060-F-N and S-RO-A1-1060-F-N) experienced more fatigue cycles than others and hence had better-represented records of the relative slip. Using the semi-logarithmic scale, the model undoubtedly captures the overall trend of the slip increment throughout the fatigue life, with a typical three-stage development: (1) the initial relative slip obtained under the first fatigue cycle; (2) a steady increase in relative slip with the number of fatigue cycle increases; and (3) a rapid climbing of relative slip as approaching to failure. This three-stage development has also been observed in many other relevant studies [15,24]. However, the proposed analytical model does not always predict the same fatigue life as obtained from the experiment (e.g., Figure 11). This could be due to the fact that regions near the free end usually have a higher local bond strength [5,23,34], exhibiting more resistance to degradation [25], but the analytical model hypothesizes a uniform local bond stress–slip relationship along the bond line under the static load and a constant degradation law for all elements along the bond line during the fatigue cycles. This creates certain degrees of deviation of the analytical predictions using the proposed model from the experimentally obtained results.

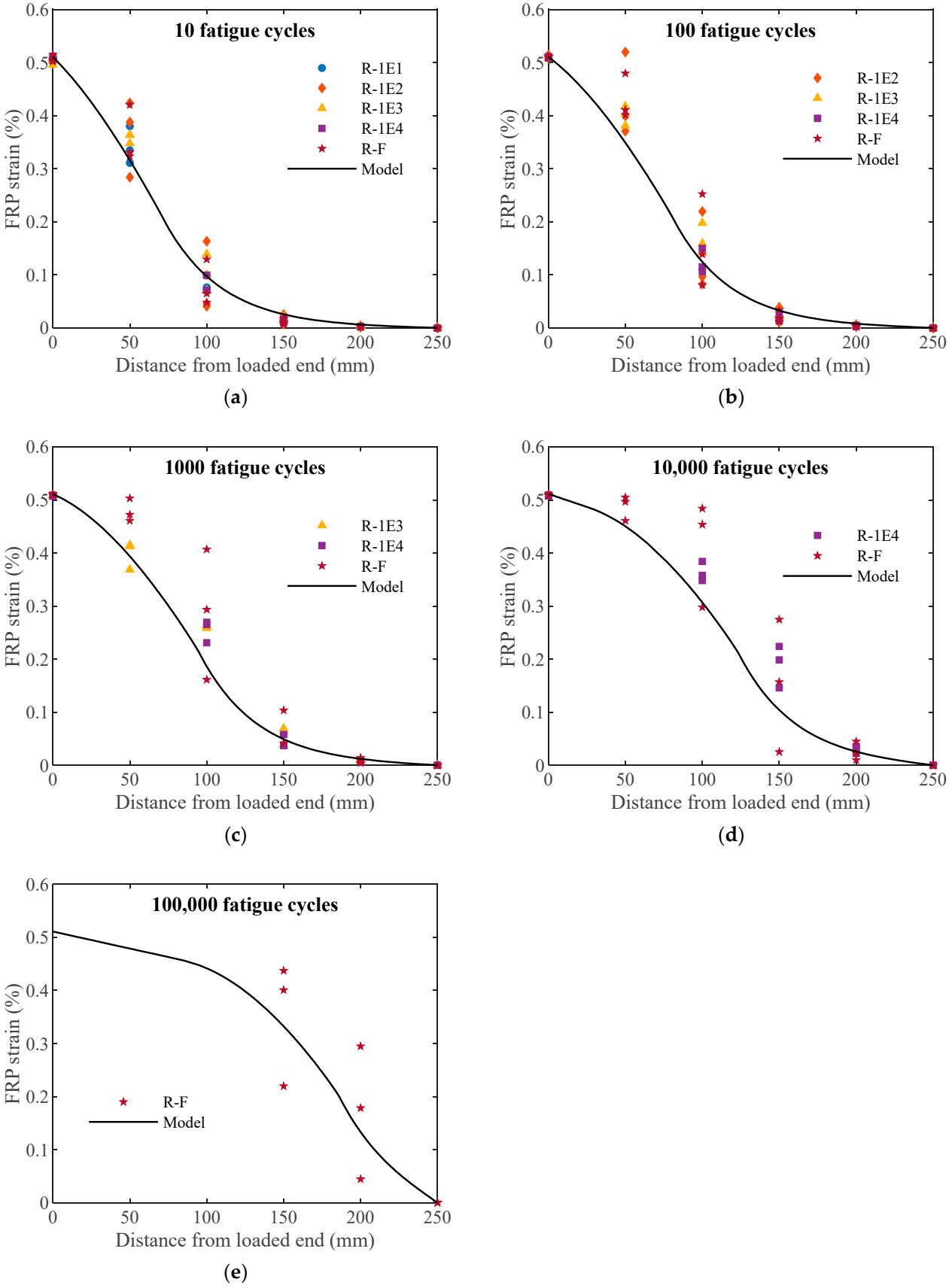


Figure 7. Comparison between test results and analytical model predictions for FRP strain distribution of CFRP rod specimens: (**a**) N = 10; (**b**) N = 100; (**c**) N = 1000; (**d**) N = 10,000; and (**e**) N = 100,000.

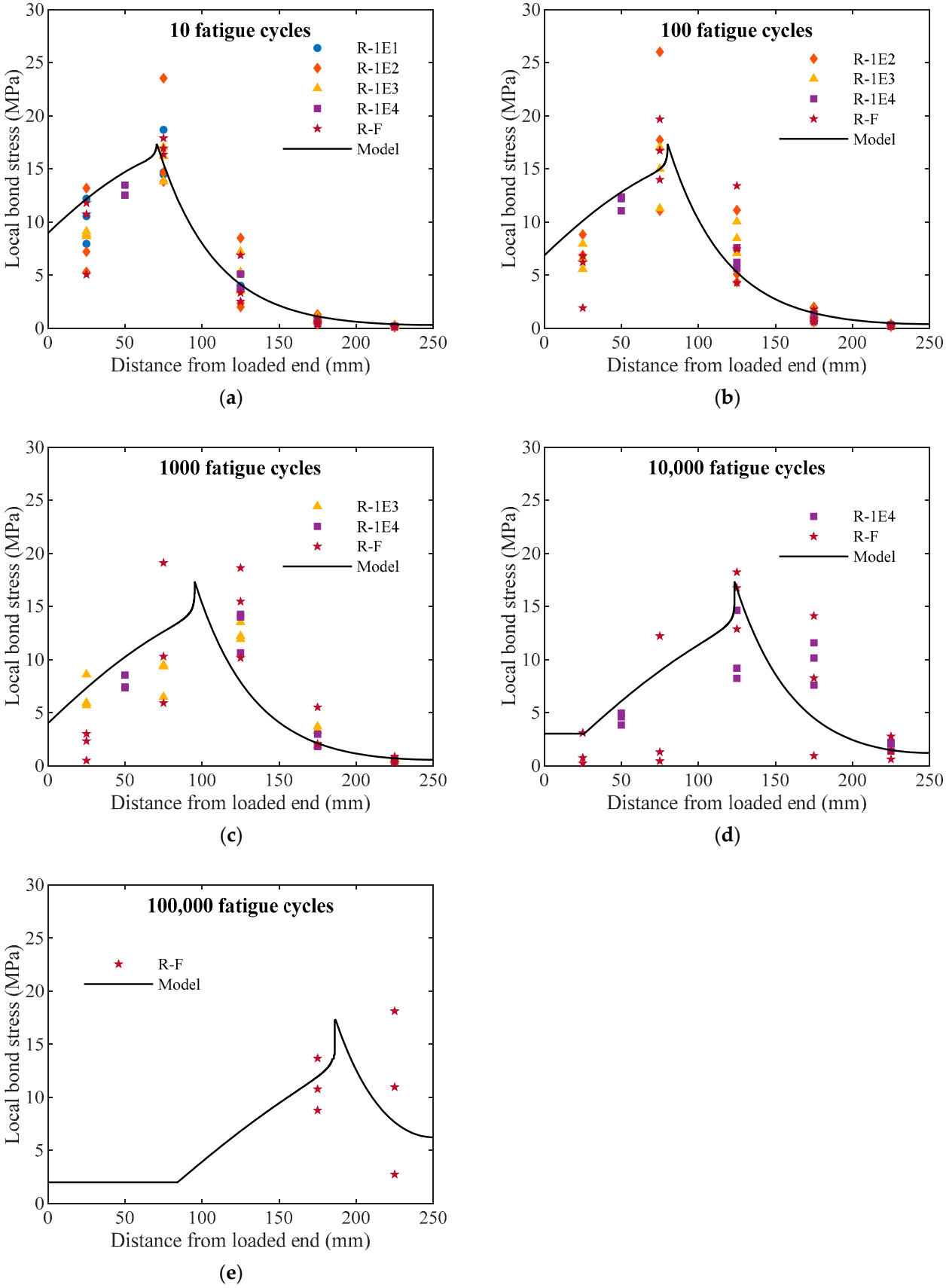


Figure 8. Comparison between test results and analytical model predictions for local bond stress distribution of CFRP rod specimens: (**a**) N = 10; (**b**) N = 100; (**c**) N = 1000; (**d**) N = 10,000; and (**e**) N = 100,000.

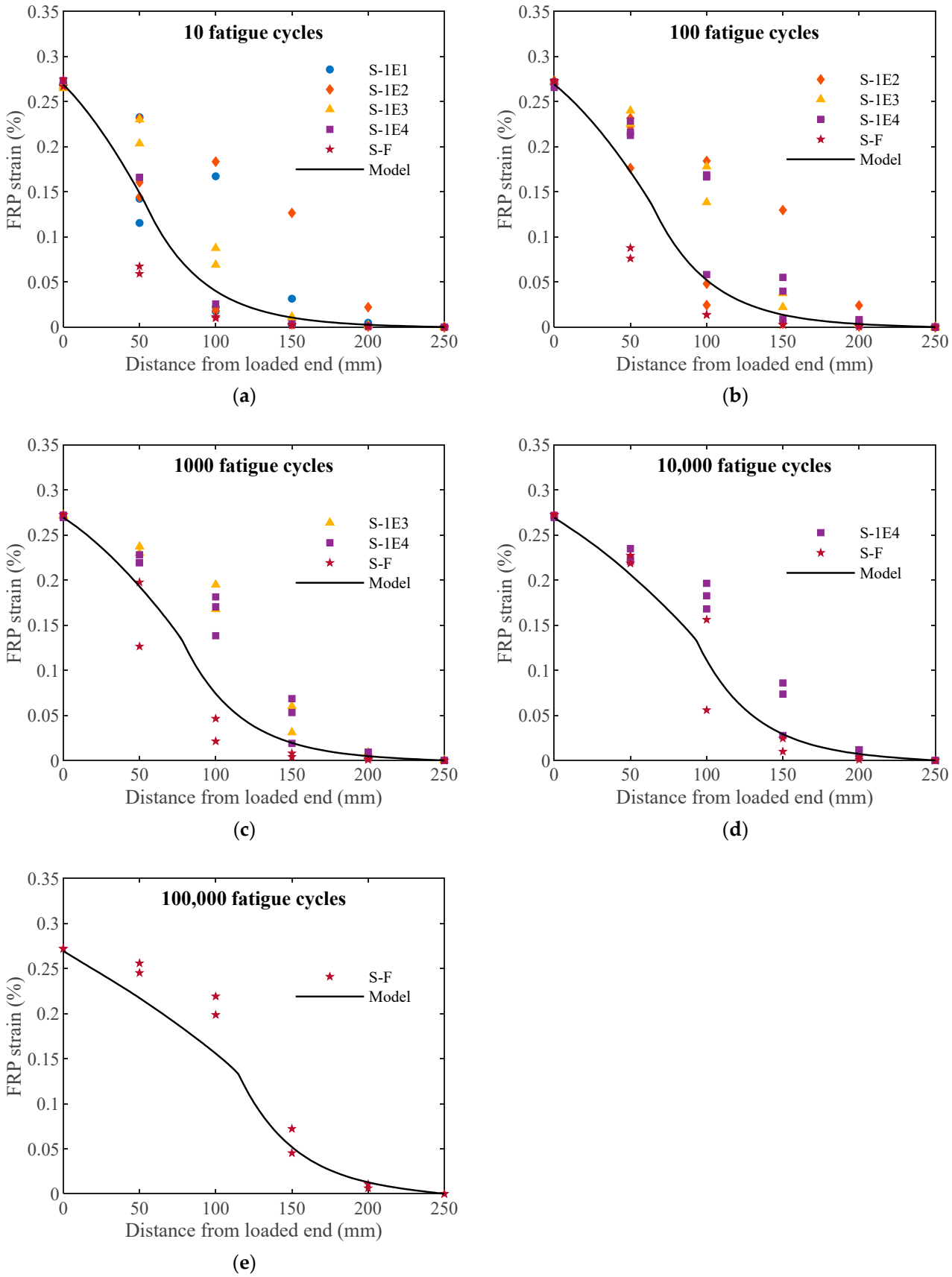


Figure 9. Comparison between test results and analytical model predictions for FRP strain distribution of CFRP strip specimens: (**a**) N = 10; (**b**) N = 100; (**c**) N = 1000; (**d**) N = 10,000; and (**e**) N = 100,000.

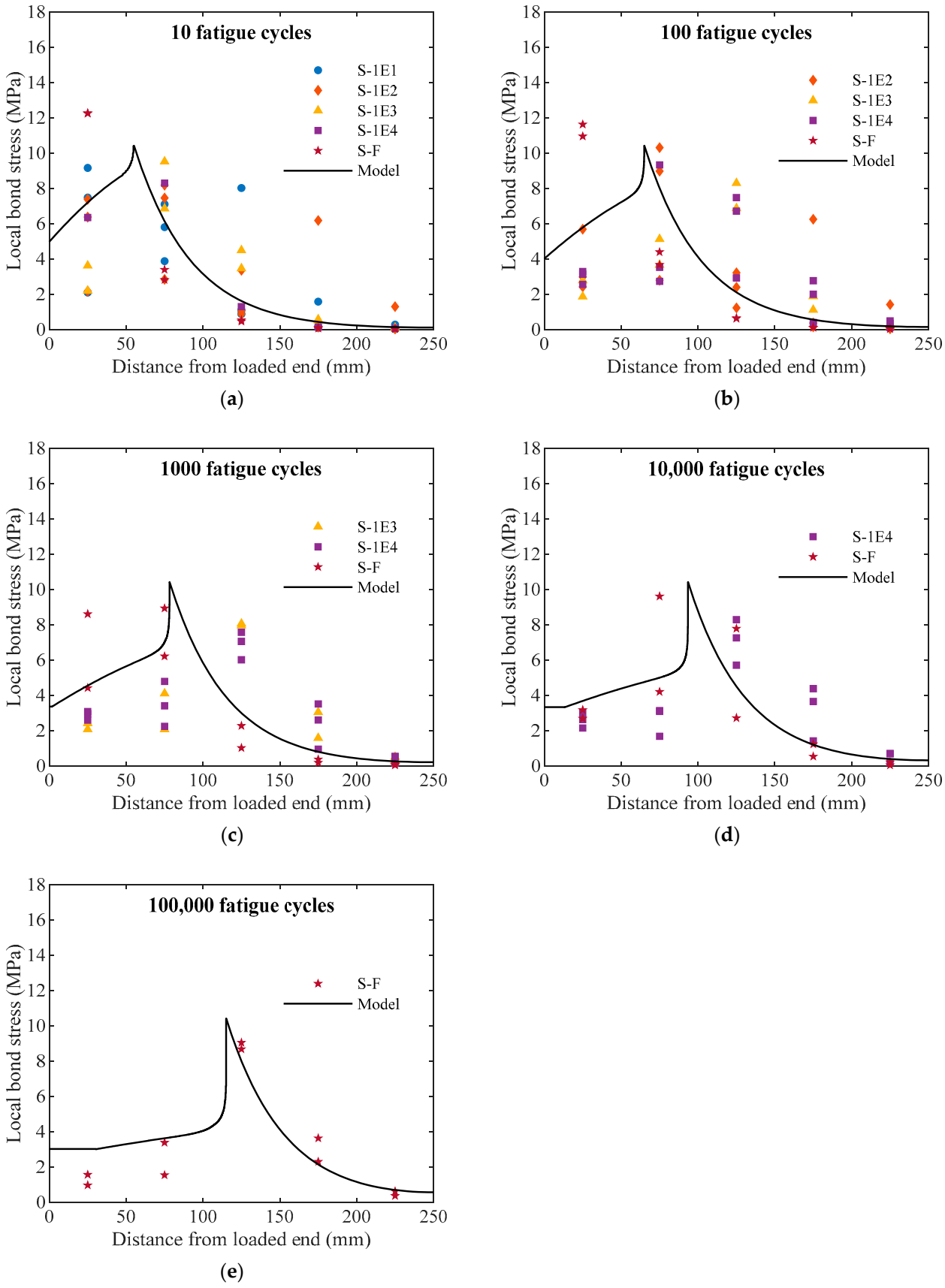


Figure 10. Comparison between test results and analytical model predictions for local bond stress distribution of CFRP strip specimens: (**a**) N = 10; (**b**) N = 100; (**c**) N = 1000; (**d**) N = 10,000; and (**e**) N = 100,000.

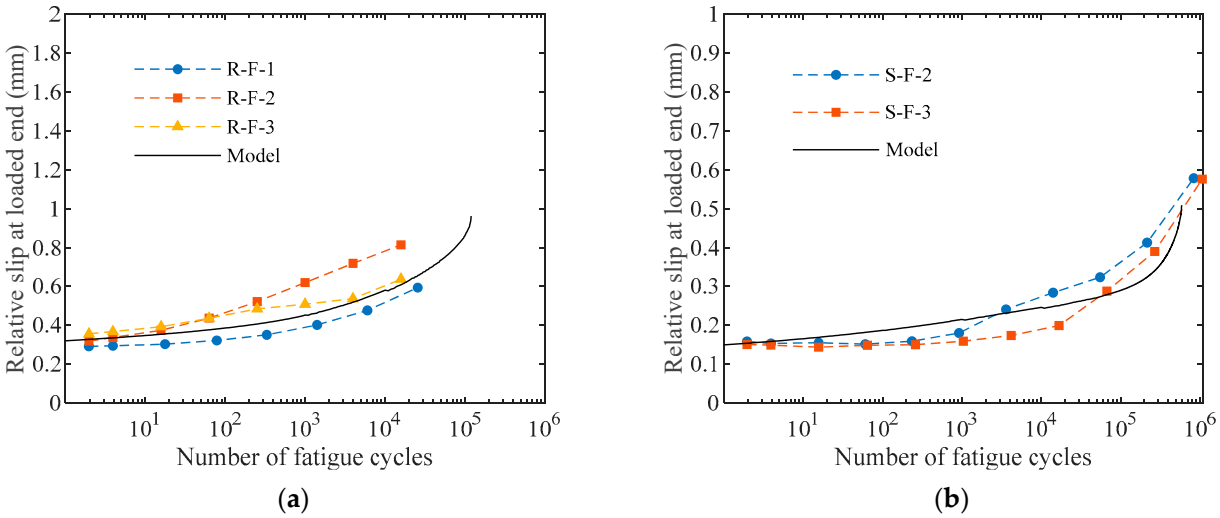


Figure 11. Comparison between test results and analytical model predictions for relative slip at the loaded end: (**a**) CFRP rod specimens; and (**b**) CFRP strip specimens.

4. Parametric Study

Using the proposed analytical model, three important parameters are investigated regarding their contribution to the local bond behavior under fatigue cycles: (1) local bond strength τ_f with a fixed residual bond strength ratio τ_r/τ_f; (2) residual bond strength ratio τ_r/τ_f; and (3) Young's modulus of FRP reinforcement. The former two parameters are critical to the bond performance of NSM FRP-to-concrete bonded joints, while the last one determines the axial stiffness of the FRP material. All other geometric information, material properties and degradation laws for CFRP reinforcement remain constant. The Young's modulus of concrete is not a major concern here as previous research reported negligible influence on the bond behavior under fatigue loading [28]. Effects due to other parameters such as groove dimensions and reinforcement size require further understanding of physical behavior via additional fatigue experimental data.

4.1. Local Bond Strength

The bond development of the NSM FRP is sensitive to the local bond strength during fatigue cycles. A ±20% range of variation is selected herein based on the original local bond strength of τ_f = 10.42 MPa with the same fatigue load range applied (i.e., 10–60% of the static pull-out force P_{max} = 32.6 kN). The original residual bond strength ratio τ_r/τ_f = 0.32 also remains constant for all cases selected herein. Figure 12 illustrates the local bond stress distribution by using various local bond strength, which indicates a substantial difference in the bond development under various fatigue cycles. Among all cases, the 120%τ_f case shows the strongest resistance to fatigue degradation with no debonding region occurring before 100,000 fatigue cycles. The length of the damaged bond region has a minimum increase from 39.07 mm under 10 cycles to 84.44 mm under 100,000 cycles. In contrast, for the 80%τ_f case, the debonding region occurs from the very beginning, and its damaged bond region has a maximum increase from 88.55 mm under 10 cycles [Figure 12a] to 166.8 mm under 100,000 cycles [Figure 12e]. Thus, it can be concluded that NSM FRP-to-concrete bonded joints can greatly benefit from a higher local bond strength where the damaged zone is more localized to the loaded end with a slower bond development under fatigue cycles.

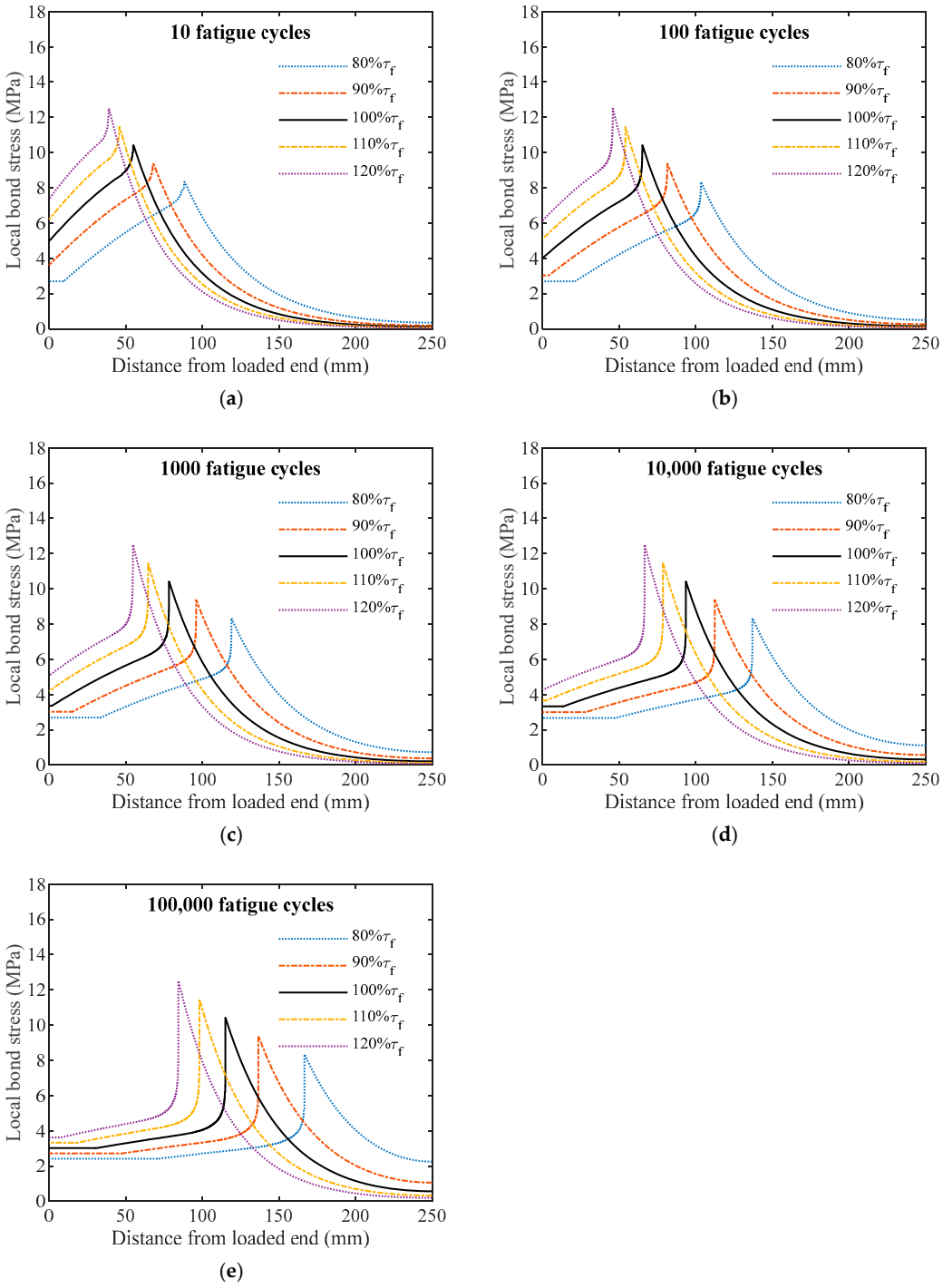


Figure 12. Influence of local bond strength on the bond behavior under fatigue cycles: (**a**) N = 10; (**b**) N = 100; (**c**) N = 1000; (**d**) N = 10,000; and (**e**) N = 100,000.

4.2. Residual Bond Strength Ratio

The residual bond strength ratio τ_r/τ_f affects the post-softening behavior of the bond development based on the trilinear local bond stress–slip model. By varying the residual bond strength ratio τ_r/τ_f from 80, 90, 100, 110 to 120% of its original magnitude (i.e., 0.32 for CFRP strip specimens) while all other parameters remain unchanged, the local bond stress distribution throughout the fatigue cycles up to 100,000 of these cases is presented in Figure 13. It can be seen that the difference in the local bond stress distribution among these cases is exceedingly small under 10 fatigue cycles [Figure 13a] and increases slightly under 100 fatigue cycles [Figure 13b]. However, after the debonding region occurs

over 1000 fatigue cycles, the difference becomes more significant and continues to grow as the number of fatigue cycles increases. At the end of 100,000 fatigue cycles, the 80% (τ_r/τ_f) case has a damaged region of 131.6 mm, while the 120% (τ_r/τ_f) case has a smaller length of 104 mm [Figure 13e]. Therefore, the residual bond strength ratio τ_r/τ_f has little influence on the local bond behavior at early fatigue cycles but affects more on the post-softening behavior of the bonded joint after debonding.

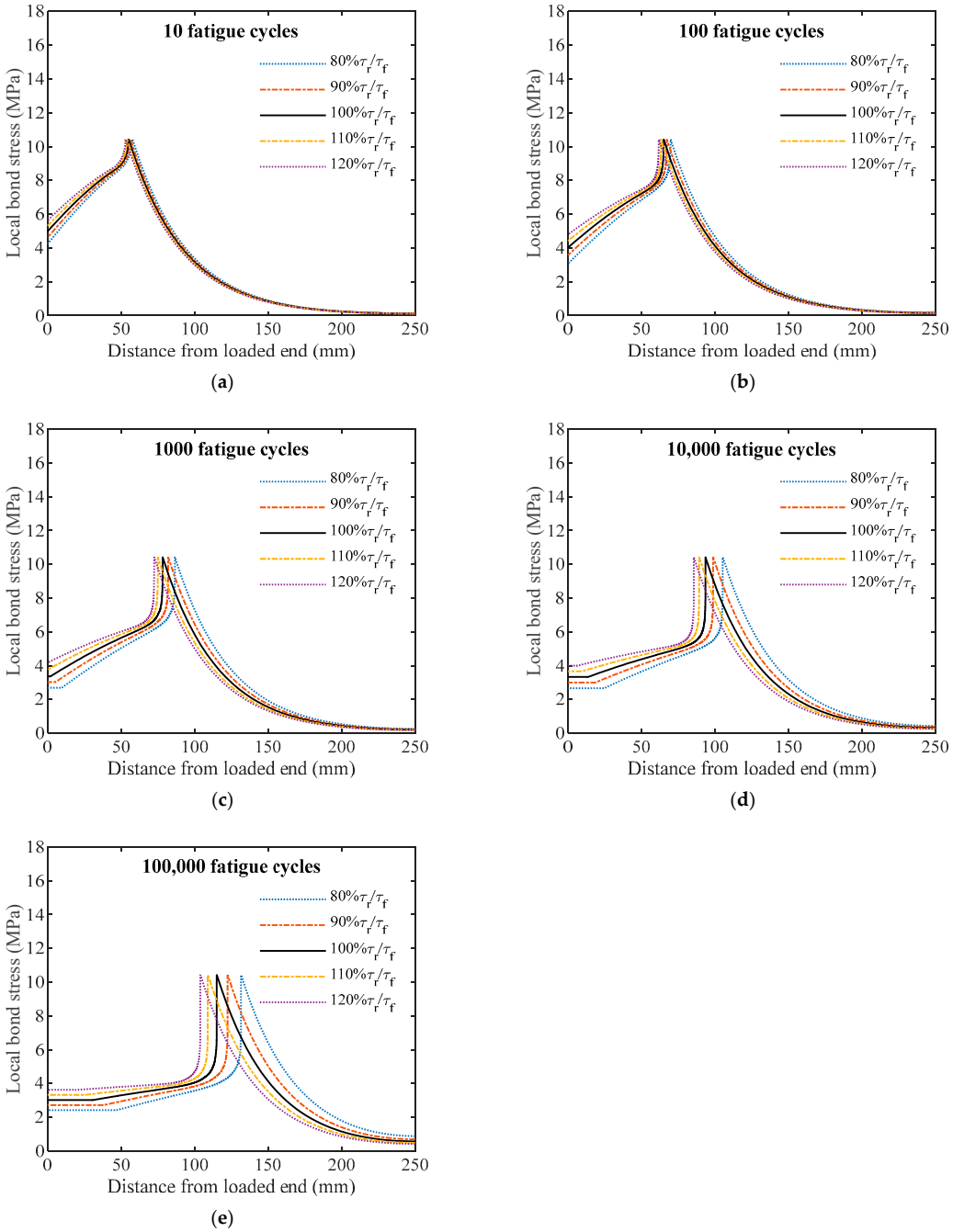


Figure 13. Influence of the residual bond strength ratio on the bond behavior under fatigue cycles: (**a**) N = 10; (**b**) N = 100; (**c**) N = 1000; (**d**) N = 10,000; and (**e**) N = 100,000.

4.3. Young's Modulus of FRP Reinforcement

In this study, the Young's modulus E_f of FRP reinforcement is allowed to vary 80, 90, 100, 110 and 120% of the original value (i.e., 168.22 GPa). Figure 14 shows a relatively stable effect caused by E_f throughout the fatigue cycles. For example, the distance between the peak local bond stress of 80%E_f and 120%E_f cases is 23.45 mm [Figure 14a] at the end of

10 fatigue cycles. It increases only slightly to 28.6 mm at the end of 100,000 fatigue cycles [Figure 14e]. This observation is expected because, unlike the local bond strength τ_f and the residual bond strength τ_r, which degrade under fatigue cycles, E_f is assumed to be constant in the proposed model. Its influence on the bond performance is thus less dependent on the number of fatigue cycles.

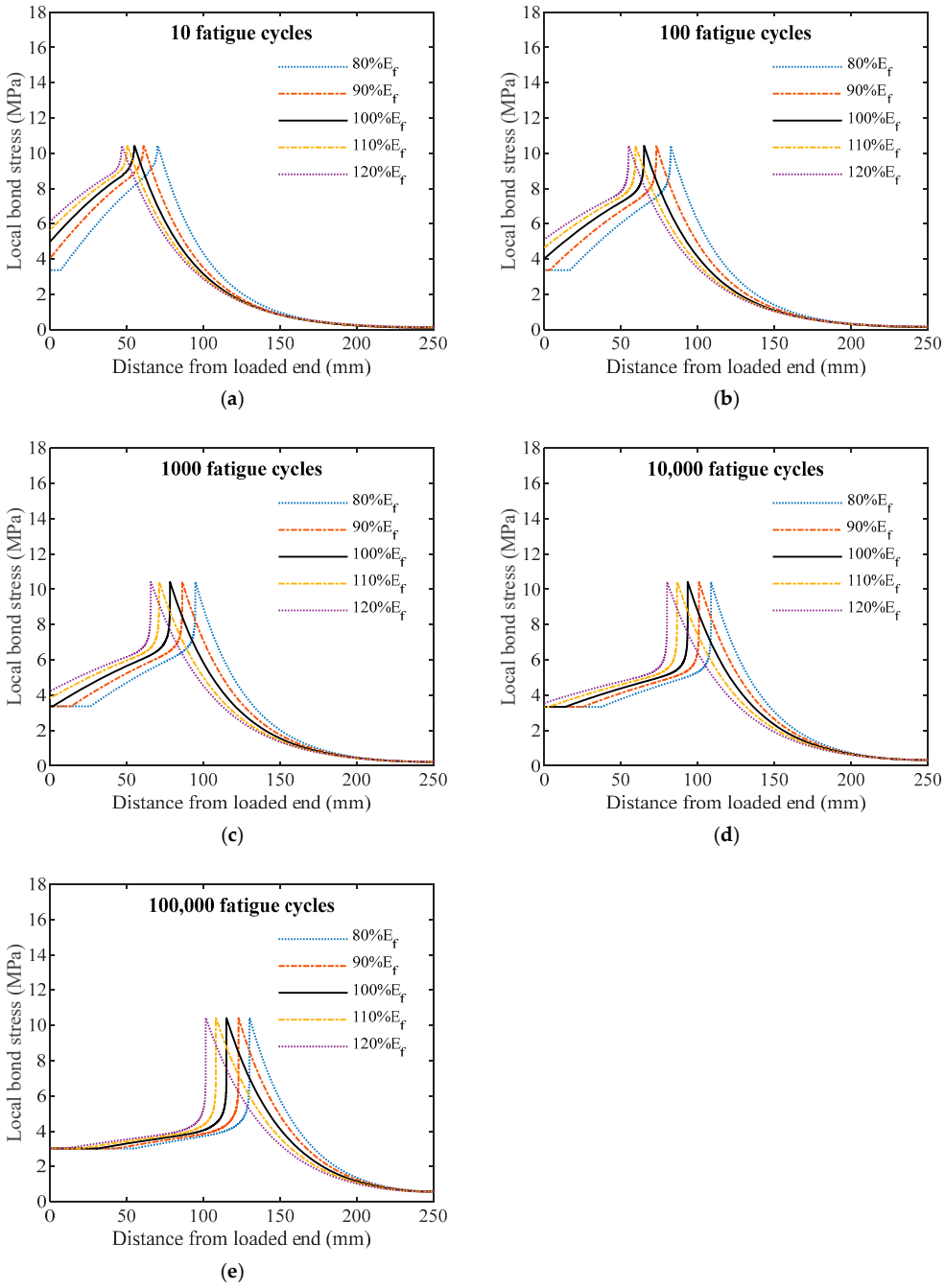


Figure 14. Influence of Young's modulus of NSM FRP reinforcement on the bond behavior under fatigue cycles: (**a**) N = 10; (**b**) N = 100; (**c**) N = 1000; (**d**) N = 10,000; and (**e**) N = 100,000.

5. Conclusions

This research proposed an analytical model based on a trilinear local bond stress–slip relationship to simulate the local bond behavior of NSM FRP-to-concrete bonded joints under fatigue cycles. Local bond degradation laws for both CFRP rod and strip specimens were obtained from a series of post-fatigue direct pull-out tests and were used to provide

the fundamental principle of the bond development under fatigue loading in the model. The mechanism of the propagation of the damaged bond region and the migration of peak local bond stress was described through an algorithm framework based on the Matlab program in combination with the FEM approach. The analytical predictions were also compared with the experimental results, followed by a set of parametric studies. The following conclusions can be drawn based on the current study:

- The discretization of the bond line into finite elements provides the maximum flexibility of managing the local bond properties at different stages of bond development. The proposed analytical model has been proven to be efficient in predicting the overall local bond degradation behavior under fatigue cycles as well as the FRP strain, local bond stress, and relative slip as compared with the experimental data;
- In some cases, the proposed model underestimates the local bond performance near the free end and predicts a lower fatigue cycle to failure. This is mainly due to the adopted hypothesis on a uniform local bond stress–slip relationship and a constant degradation law for all elements along the bond line during fatigue cycles; and
- Based on the parametric study, the local bond strength has the most significant effect on the local bond development throughout the fatigue life of specimens. The residual bond strength ratio influences more on the post-softening behavior of the bond, consequently causing more effect at higher numbers of fatigue cycles. In contrast, the Young's modulus of FRP reinforcement has a relatively stable influence on the local bond behavior and is less sensitive to the number of fatigue cycles.

Author Contributions: Conceptualization, X.W. and L.C.; methodology, X.W. and L.C.; software, X.W.; validation, X.W. and L.C.; formal analysis, X.W. and L.C.; investigation, X.W. and L.C.; resources, X.W. and L.C.; data curation, X.W.; writing—original draft preparation, X.W.; writing—review and editing, X.W. and L.C.; visualization, X.W. and L.C.; supervision, L.C.; project administration, L.C.; funding acquisition, L.C. All authors have read and agreed to the published version of the manuscript.

Funding: This research received no external funding.

Data Availability Statement: The original contributions presented in this study are included in the article. Further inquiries can be directed to the corresponding authors.

Conflicts of Interest: Author Xun Wang was employed by the company CHEC USA Inc. The remaining authors declare that this research was conducted in the absence of any commercial or financial relationships that could be construed as a potential conflict of interest.

Notation

The following symbols are used in this paper:

A_c	cross-sectional area of concrete block (mm^2);
A_f	cross-sectional area of NSM FRP reinforcement (mm^2);
${C_1}^i$, ${C_2}^i$ and ${C_3}^i$	introduced constants of the ith element;
E_c	Young's modulus of concrete block (MPa);
E_f	Young's modulus of NSM FRP reinforcement (MPa);
i	index of the finite element;
L	bond length (mm);
L_d	debonding length (mm);
${L_d}^1$	debonding length at the 1st fatigue cycle (mm);
${L_d}^k$	debonding length at the kth fatigue cycle (mm);
L_f	bond failure limit (mm);
L_p	perimeter of the failure plane (mm);
L_s	softening length (mm);
${L_s}^1$	softening length at the 1st fatigue cycle (mm);
${L_s}^k$	softening length at the kth fatigue cycle (mm);

n_1, n_2, n_3	notation to indicate the number of elements in different bond regions;
N	number of fatigue cycles;
P_f	pull-out force of specimen in the experiment (kN);
P_{max}	magnitude of upper limit of the applied fatigue load range (N);
T_{force}	force tolerance (N);
T_{slip}	slip tolerance (mm);
x	distance from the free end (mm);
x_0	free end of the bond line (mm);
x_{i-1}, x_i	start and end coordinate of the ith element (mm);
x_{n1}	boundary between elastic and softening bond region at the 1st fatigue cycle (mm);
x_{n2}	boundary between elastic and softening bond region at the 1st fatigue cycle (mm);
x_{n3}	loaded end of the bond line at the 1st fatigue cycle (mm);
δ	relative slip between FRP reinforcement and concrete block (mm);
δ_1	relative slip corresponding to the local bond strength (mm);
δ_f	relative slip at debonding (mm);
λ, ${\lambda_1}^i$, ${\lambda_2}^i$	introduced symbols to simplify the expression;
σ_f	stress of NSM FRP reinforcement (MPa);
τ_{avg}	average bond strength (MPa);
τ_f	local bond strength between the FRP reinforcement and concrete (MPa);
$\tau_{f,static}$	static local bond strength (MPa);
${\tau_f}^i(N)$	local bond strength for the ith finite element at the Nth fatigue cycle (MPa);
$\tau_i(\delta)$	local bond stress–slip relationship for the ith finite element (MPa);
τ_r	residual bond strength between the FRP reinforcement and concrete (MPa);
$\tau_{r,static}$	static residual bond strength (MPa); and
${\tau_r}^i(N)$	residual local bond strength for the ith finite element at the Nth fatigue cycle (MPa).

References

1. De Lorenzis, L.; Teng, J.G. Near-surface mounted FRP reinforcement: An emerging technique for strengthening structures. *Compos. Part B Eng.* **2007**, *38*, 119–143. [CrossRef]
2. Coelho, M.R.F.; Sena-Cruz, J.M.; Neves, L.A.C. A review on the bond behavior of FRP NSM systems in concrete. *Constr. Build. Mater.* **2015**, *93*, 1157–1169. [CrossRef]
3. Galati, D.; De Lorenzis, L. Effect of construction details on the bond performance of NSM FRP bars in concrete. *Adv. Struct. Eng.* **2009**, *12*, 683–700. [CrossRef]
4. Soliman, S.M.; El-Salakawy, E.; Benmokrane, B. Bond performance of near-surface-mounted FRP bars. *J. Compos. Constr.* **2011**, *15*, 103–111. [CrossRef]
5. Lee, D.; Cheng, L.; Yan-Gee Hui, J. Bond characteristics of various NSM FRP reinforcements in concrete. *J. Compos. Constr.* **2013**, *17*, 117–129. [CrossRef]
6. Khshain, N.T.; Al-Mahaidi, R.; Abdouka, K. Bond behaviour between NSM CFRP strips and concrete substrate using single-lap shear testing with epoxy adhesive. *Compos. Struct.* **2015**, *132*, 205–214. [CrossRef]
7. Torres, L.; Sharaky, I.A.; Barris, C.; Baena, M. Experimental study of the influence of adhesive properties and bond length on the bond behaviour of NSM FRP bars in concrete. *J. Civ. Eng. Manag.* **2016**, *22*, 808–817. [CrossRef]
8. Sharaky, I.A.; Baena, M.; Barris, C.; Sallam, H.E.M.; Torres, L. Effect of axial stiffness of NSM FRP reinforcement and concrete cover confinement on flexural behaviour of strengthened RC beams: Experimental and numerical study. *Eng. Struct.* **2018**, *173*, 987–1001. [CrossRef]
9. Zhang, S.S.; Yu, T.; Chen, G.M. Reinforced concrete beams strengthened in flexure with near-surface mounted (NSM) CFRP strips: Current status and research needs. *Compos. Part B Eng.* **2017**, *131*, 30–42. [CrossRef]

10. Fahmy, M.F.M.; Wu, Z. Exploratory study of seismic response of deficient lap-splice columns retrofitted with near surface-mounted basalt FRP bars. *J. Struct. Eng.* **2016**, *142*, 04016020. [CrossRef]
11. Yoshitake, I.; Kim, Y.J.; Yumikura, K.; Hamada, S. Moving-wheel fatigue for bridge decks strengthened with CFRP strips subject to negative bending. *J. Compos. Constr.* **2010**, *14*, 784–790. [CrossRef]
12. Al-Jaberi, Z.; Myers, J.J.; ElGawady, M.A. Pseudo-static cyclic loading comparison of reinforced masonry walls strengthened with FRCM or NSM FRP. *Constr. Build. Mater.* **2018**, *167*, 482–495. [CrossRef]
13. Yun, Y.; Wu, Y.F.; Tang, W.C. Performance of FRP bonding systems under fatigue loading. *Eng. Struct.* **2008**, *30*, 3129–3140. [CrossRef]
14. Carloni, C.; Subramaniam, K.V. Investigation of sub-critical fatigue crack growth in FRP/concrete cohesive interface using digital image analysis. *Compos. Part B Eng.* **2013**, *51*, 35–43. [CrossRef]
15. Fernandes, P.M.G.; Silva, P.M.; Sena-Cruz, J. Bond and flexural behavior of concrete elements strengthened with NSM CFRP laminate strips under fatigue loading. *Eng. Struct.* **2015**, *84*, 350–361. [CrossRef]
16. Quattlebaum, J.B.; Harries, K.A.; Petrou, M.F. Comparison of three flexural retrofit systems under monotonic and fatigue loads. *J. Bridge Eng.* **2005**, *10*, 731–740. [CrossRef]
17. Aidoo, J.; Harries, K.A.; Petrou, M.F. Full-scale experimental investigation of repair of reinforced concrete interstate bridge using CFRP materials. *J. Bridge Eng.* **2006**, *11*, 350–358. [CrossRef]
18. Sena-Cruz, J.M.; Barros, J.A.O.; Coelho, M.R.F.; Silva, L.F.F.T. Efficiency of different techniques in flexural strengthening of RC beams under monotonic and fatigue loading. *Constr. Build. Mater.* **2012**, *29*, 175–182. [CrossRef]
19. Charalambidi, B.G.; Rousakis, T.C.; Karabinis, A.I. Fatigue behavior of large-scale reinforced concrete beams strengthened in flexure with fiber-reinforced polymer laminates. *J. Compos. Constr.* **2016**, *20*, 04016035. [CrossRef]
20. Badawi, M.; Soudki, K. Fatigue behavior of RC beams strengthened with NSM CFRP rods. *J. Compos. Constr.* **2009**, *13*, 415–421. [CrossRef]
21. Wahab, N.; Soudki, K.A.; Topper, T. Experimental investigation of bond fatigue behavior of concrete beams strengthened with NSM Prestressed CFRP Rods. *J. Compos. Constr.* **2012**, *16*, 685–692. [CrossRef]
22. Oudah, F.; El-Hacha, R. Performance of RC beams strengthened using prestressed NSM-CFRP strips subjected to fatigue loading. *J. Compos. Constr.* **2012**, *16*, 300–307. [CrossRef]
23. Chen, C.; Cheng, L. Fatigue bond characteristics and degradation of near-surface mounted CFRP rods and strips in concrete. *J. Compos. Constr.* **2016**, *20*, 04015066. [CrossRef]
24. Al-Saadi, N.T.K.; Al-Mahaidi, R. Fatigue performance of NSM CFRP strips embedded in concrete using epoxy adhesive. *Compos. Struct.* **2016**, *154*, 419–432. [CrossRef]
25. Wang, X.; Cheng, L. Full-range fatigue behavior of NSM CFRP-to-concrete bonded joints. *Eng. Struct.* **2023**, *295*, 116812. [CrossRef]
26. Yuan, H.; Wu, Z.; Yoshizawa, H. Theoretical solutions on interfacial stress transfer of externally bonded steel/composite laminates. *Struct. Eng. Eng.* **2001**, *675*, 27–39. [CrossRef]
27. Yuan, H.; Teng, J.G.; Seracino, R.; Wu, Z.S.; Yao, J. Full-range behavior of FRP-to-concrete bonded joints. *Eng. Struct.* **2004**, *26*, 553–565. [CrossRef]
28. Chen, C.; Cheng, L. Theoretical solution to fatigue bond stress distribution of NSM FRP reinforcement in concrete. *Compos. Part B Eng.* **2016**, *99*, 453–464. [CrossRef]
29. Seracino, R.; Raizal Saifulnaz, M.R.; Oehlers, D.J. Generic debonding resistance of EB and NSM plate-to-concrete joints. *J. Compos. Constr.* **2007**, *11*, 62–70. [CrossRef]
30. Oehlers, D.J.; Haskett, M.; Wu, C.; Seracino, R. Embedding NSM FRP plates for improved IC debonding resistance. *J. Compos. Constr.* **2008**, *12*, 635–642. [CrossRef]
31. Ceroni, F.; Pecce, M.; Bilotta, A.; Nigro, E. Bond behavior of FRP NSM systems in concrete elements. *Compos. Part B Eng.* **2012**, *43*, 99–109. [CrossRef]
32. Dai, J.; Ueda, T.; Sato, Y. Development of the nonlinear bond stress-slip model of fiber reinforced plastics sheet-concrete interfaces with a simple method. *J. Compos. Constr.* **2005**, *9*, 52–62. [CrossRef]
33. Zhang, S.S.; Teng, J.G.; Yu, T. Bond-slip model for CFRP strips near-surface mounted to concrete. *Eng. Struct.* **2013**, *56*, 945–953. [CrossRef]
34. Wang, X.; Cheng, L. Bond characteristics and modeling of near-surface mounted CFRP in concrete. *Compos. Struct.* **2021**, *255*, 113011. [CrossRef]

Disclaimer/Publisher's Note: The statements, opinions and data contained in all publications are solely those of the individual author(s) and contributor(s) and not of MDPI and/or the editor(s). MDPI and/or the editor(s) disclaim responsibility for any injury to people or property resulting from any ideas, methods, instructions or products referred to in the content.